ORIGINAL PAPER

Experiment and numerical simulation of overburden and surface damage law in shallow coal seam mining under the gully

Jiangbo Wei[1,2,3] · Shuangming Wang[1,2,3] · Shijie Song[1,2,3] · Qiang Sun[1,2,3] · Tian Yang[1,2,3]

Abstract

Safe and environmentally friendly coal mining in loess gully regions is one of the most popular research topics in the coal industry. In this study, the development law of surface cracks is interpreted and analyzed by unmanned aerial vehicle (UAV) remote sensing technology. The macroscopic and microscopic characteristics and laws governing rock-mass damage, such as overburden failure, fracture development, force chain evolution, and fragment distribution, are simulated and analyzed, and their results are compared with field drilling data for verification. The results show that the surface cracks are predominantly linear "step cracks" parallel to the cut direction, with an average spacing of 10 m. For the first time, the overburden exhibits cyclic deformation damage characteristics of "separation of strata—caved and disappearance of separation—generation of high-level separation." The height of the caving zone is 9.9 m, the periodic caving step distance is 10 m, and the water-flowing fissure penetrates to the surface. Vertical deformation of the overburden rock and the ground surface is M-shaped, with a maximum surface subsidence of 1.6 m. In the future, the research results can provide theoretical guidance for overburden and surface damage prevention and control of shallow coal seam mining under the gully in the Northern Shaanxi mining area, China.

Introduction

Coal resources account for more than 50% of primary energy consumption and production in China. Coal resources are widely distributed and heavily overlap with agricultural cultivated land and ecologically sensitive areas. The exploitation of coal resources has caused serious harm to China's ecological and cultivated land environment, especially in the ecologically fragile area of Western China, where intensive extraction of shallow coal seams has accelerated the deterioration of the ecological environment (Bai et al. 2019).

China's coal mining has gradually evolved from the simple pursuit of high efficiency to green mining and integrated ecological environment development as science, technology, and the economy have advanced (Fig. 1).

Coal mining has caused a series of geological and ecological concerns, including surface cracks, land subsidence, reductions in surface water and spring areas, declines in groundwater levels, and vegetation degradation (Wang et al. 2020a; Liu et al. 2018). Additionally, the development of mining slope cracks will induce slope instability, which will result in secondary mine geological disasters (Xu et al. 2016; Tang et al. 2019). However, the primary reason of these adverse external impacts is mining's large-scale and high-strength deformation and fracture development of the overburden. Therefore, an in-depth study of overburden deformation damage and fracture development characteristics caused by coal mining disturbance, revealing the mechanism of goaf geological disasters and environmental damage, has significant theoretical and practical implications for achieving safe mines, coal mining water conservation, and surface ecological environmental protection.

✉ Shuangming Wang
mtlskcdzyjy@163.com

1 College of Geology and Environment, Xi'an University of Science and Technology, Xi'an, Shaanxi 710054, China

2 Geological Research Institute for Coal Green Mining, Xi'an University of Science and Technology, Xi'an, Shaanxi 710054, China

3 Shaanxi Provincial Key Laboratory of Geological Support for Coal Green Exploitation, Xi'an University of Science and Technology, Xi'an, Shaanxi 710054, China

Fig. 1 Development course of coal mining in China
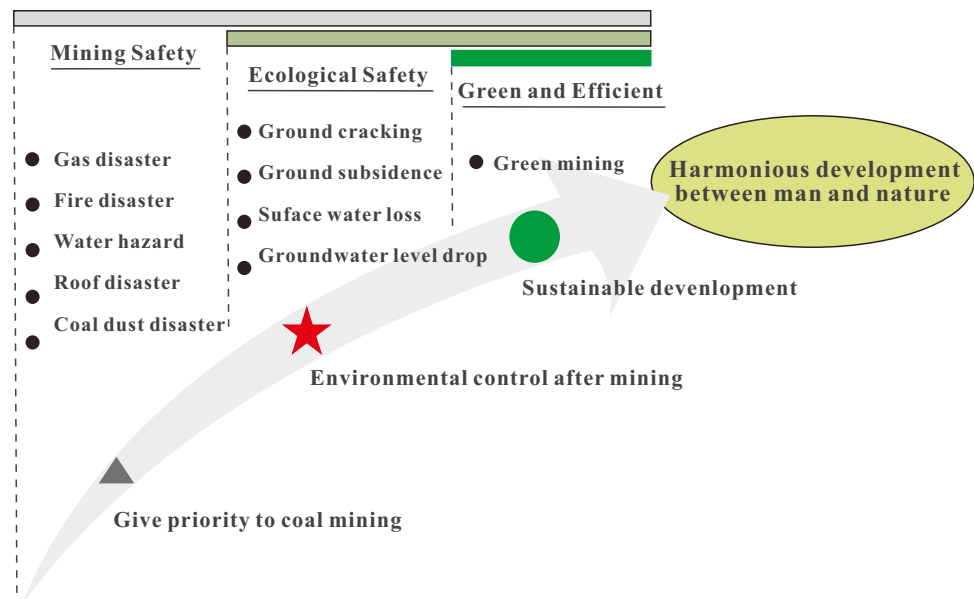
In view of the numerous ecological and geological environmental challenges associated with coal exploitation in ecologically sensitive areas of Western China (Guo et al. 2019), many scholars have carried out substantial research on the rules of overburden damage, surface deformation, fractures, and separation development. Furthermore, the relevant research on mining damage is conducted through field investigation and monitoring (Liu et al. 2019a, b; Wu et al. 2019; Yang et al. 2019), theoretical analysis (Majdi et al. 2012; Guo et al. 2018, 2021; Wang et al. 2019), indoor test (Zhu et al. 2018; Xu et al. 2019), and numerical test (Wang et al. 2017; Cao et al. 2018; Kong et al. 2019; Sun et al. 2019). Although field monitoring research is very authentic and reliable, performing microscale analysis is challenging and necessitates significant human resources, material, and financial resources (Mondal et al. 2020). Rezaei et al. (2015a, b, 2018) developed a time-independent energy analysis model based on the strain energy balance theory and utilized it to compute the height of the destressed zone above the goaf roof caused by longwall mining, which was then verified by mathematical statistics. Although the theoretical analysis is simple and straightforward, it requires establishing numerous assumptions and simplifying geological factors and characteristics. Complex geological factors are difficult to evaluate thoroughly, resulting in huge errors, and the dynamic deformation process of overburden cannot be analyzed. Similar indoor material simulation tests can compensate for the aforementioned limitations due to their short testing period, ease control of experimental settings, and cost efficiency. Furthermore, numerical tests are more convenient and flexible than similar tests and can take into account the influence of complex geological factors (Behera et al. 2019). The comprehensive comparative analysis demonstrates that similar model tests and numerical simulation tests are effective methods for dynamic analysis of deformation damage and fracture development in mining overburden, as they can not only verify the accuracy of the field measurement results but also obtain data and dynamic development rules that are not theoretically or practically available.

In China, Northern Shaanxi is characterized by a typical loess ridge and hill landform with intricate terrain and ravines. In recent years, research on mining-induced overburden damage has primarily focused on the influence of internal factors such as the structure and type of the rock-soil mass on the deformation characteristics and fracture development law of overburden in goafs (Bai et al. 2017; Zhang et al. 2019), while little attention paid to external factors such as surface morphology (Gao et al. 2019). Based on previous field observations, the overburden deformation damage and surface damage characteristics are impacted not only by the type and structure of the overburden rock, but also by the topography and geomorphology. For example, the trench bottom is shallowly buried, yet the mining damage is severe (Jiang et al. 2017). The mining-induced deformation of the slope has a certain amplification effect (Wang et al. 2013). Therefore, it is imperative to investigate the overlying rock failure and crack development law under the influence of topographical factors following mining. The working face of Caigou in the Anshan minefield serves as an excellent illustration. This example simulates and analyzes the macroscopic and microscopic properties and rules, including overburden failure, fracture development, force chain evolution, and fragment distribution. The research findings can provide theoretical support for reducing ecological damage and preventing and controlling geological disasters caused by other trench working faces or similar
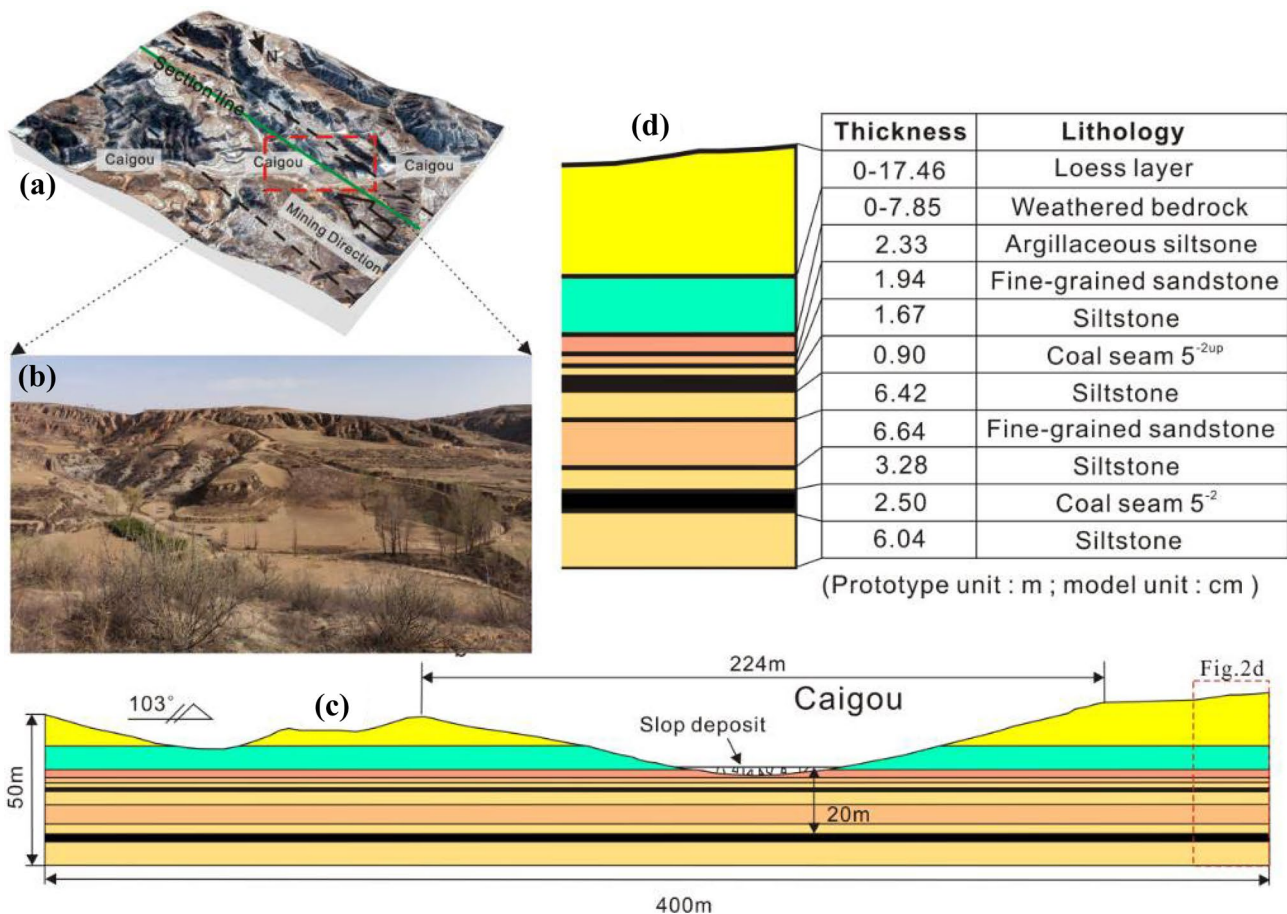
geological conditions in the mining area, as well as technical guidance for achieving coordinated resource development and environmental protection in the mining area.

Geological overview and field characteristics

The study area is sited in the Miaohagu mining area, Miaogoumen town, Fugu County, Yulin city, Shaanxi Province, China. The average annual temperature and rainfall are 9.1 ℃ and 433.1 mm, respectively. From July to September every year, rainfall is abundant, which means that flooding is frequent occurrence in the channel. The research object is the 125,203 working face in the Anshan minefield in northwestern Caigou (Fig. 2a), has loess beams and gully landforms on the surface, sparse vegetation, and serious soil erosion (Fig. 2b). The working face measures 3152×270 m in size. The main mining seam 5^{-2} is shallowly buried and roughly flat, with an average thickness of 2.5 m. Above the coal seam, there is 20 ~ 65-m-thick bedrock, which is covered by a 0 ~ 77-m-thick loose layer. The coal seam is mined using a comprehensive mechanized mining method, while the roof is managed by the natural span falling method. According to the field survey, the maximum depth of the main valley and the span in the Caigou section of the 125,203 working face are 25 m and 224 m, respectively. The vertical distance between coal seam 5^{-2} and the ditch bottom is approximately 20 m (Fig. 2c). The direct top (bottom) plate of the 5^{-2} coal seam is mainly siltstone, the main roof is fine-grained sandstone, the upper part of the bedrock is covered by Quaternary loess, and bedrock is exposed at the foot of the slope and trench bottom (Fig. 2d).

As we can know from the UAV image interpretation and field investigation results (Fig. 3), the cracks at the bottom of the trench were all developed in the working face and parallel to the cut hole. The fracture type is a "step crack" (Fig. 3f, i). The average spacing between two adjacent cracks is 10 m and the majority of the cracks are linear with a few being curved. Parallel to the cut hole, the fractures in the slope area are many arching surface cracks with a drop of about 0.5 m at the top, accompanied by a collapsed trough (Fig. 3b, c). When the slope direction is consistent with the

Thickness	Lithology
0-17.46	Loess layer
0-7.85	Weathered bedrock
2.33	Argillaceous siltsone
1.94	Fine-grained sandstone
1.67	Siltstone
0.90	Coal seam 5^{-2up}
6.42	Siltstone
6.64	Fine-grained sandstone
3.28	Siltstone
2.50	Coal seam 5^{-2}
6.04	Siltstone

(Prototype unit : m ; model unit : cm)

Fig. 2 Location map of the study area. (**a**) Remote sensing image of the mining face passing through the Caigou; (**b**) surface morphology characteristics of the Caigou; (**c**) cross-sectional profile; and (**d**) typical geological log profile of the Caigou section

Fig. 3 Development characteristics of surface fractures in Goaf
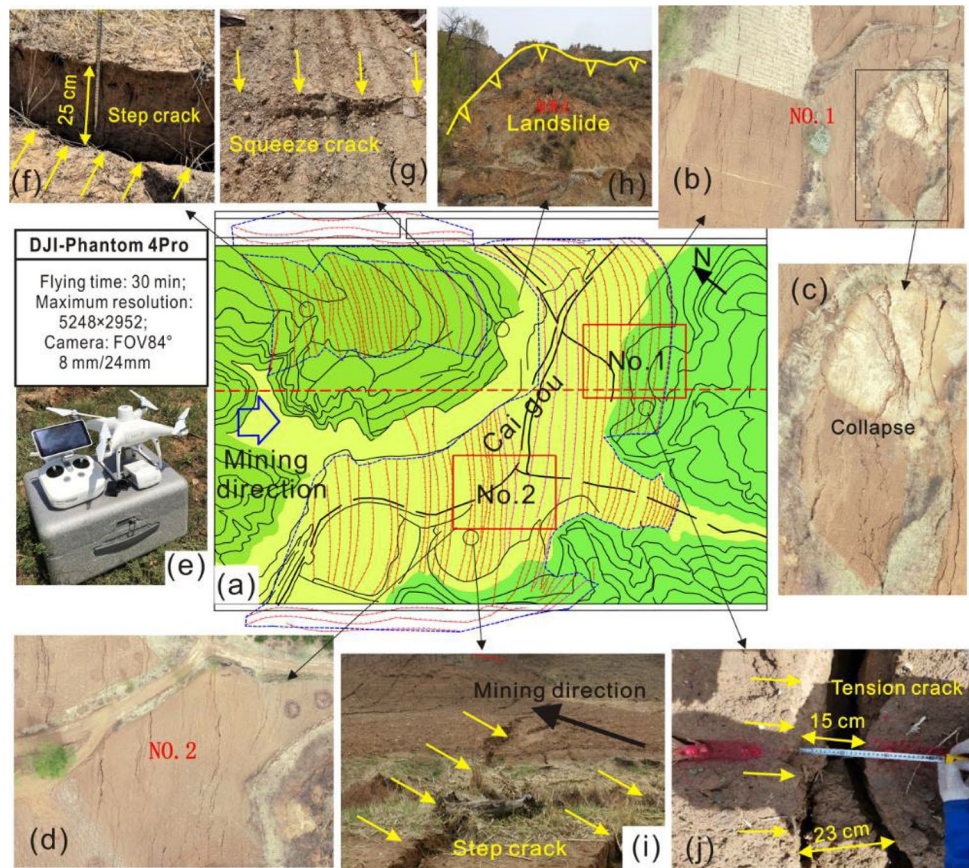
mining direction (consequent slope), several parallel cracks are produced by sliding compression on the slope surface (Fig. 3g). When the slope is in the opposite direction of the mining direction (reverse slope), numerous parallel fractures occur (Fig. 3j). Parallel to the roadway, cracks emerge on both flanks (Fig. 3a). The cracks are mostly "step cracks," the ground collapse on the slope top is serious, and both sides of the slopes are accompanied by yellow soil landslides (Fig. 3h).

Modeling building

Physical model

The geometric similarity ratio is determined as $K_L = 1:100$ after a comprehensive analysis of experiments and geological conditions of the Caigou 125,203 working face, as well as the size proportion relationship between the test device and the actual working face; and the density similarity ratio is determined as $K_\gamma = 1:1.6$ based on the properties and proportion of the selected simulation materials. Thus, the strength similarity ratio is $K_\sigma = K_L K_\gamma = 1:160$, and the time similarity ratio is $K_\sigma = \sqrt{K_L} = 10$ (Ghabraie et al. 2015; Wang et al. 2017). According to the general characteristics

of the stratigraphic structure in the area where coal measurements are taken, a Muscovite sheet is used to simulate the bedding plane between rock strata with river sand as aggregate, gypsum as cement, and white powder as filler (Wang et al. 2017).

The experimental model of overburden deformation in cross trench mining was established using the planning model physical simulation experiment system in accordance with the geological conditions of the Caigou, and the corresponding displacement monitoring points and strain monitoring speckle were arranged. A prism-free total station and VIC-3D noncontact full-field strain measurement instrument were used to monitor the displacement deformation of the overburden. The modeling process is shown in Fig. 4.

Numerical model and parameters

Since the discontinuous nature of the deformation and failure of overburden in coal seam mining, it is difficult for the continuous medium model of the finite element method to explain the discontinuous deformation phenomenon from microcrack initiation to macrofracture, as well as its internal mechanism and dynamic mechanical process. However, the particle discrete element method resolves this problem in principle (Gao et al. 2020a).

Fig. 4 Experimental process diagram. (**a**) Material weighing; (**b**) Material mixing; (**c**) Even stirring; (**d**) Material mounting and compacting; (**e**) Initial model; (**f**) Monitoring rock mass deformation by the total station; (**g**) Monitoring rock mass full-field strain by Vic-3D noncontact full-field strain measurement instrument
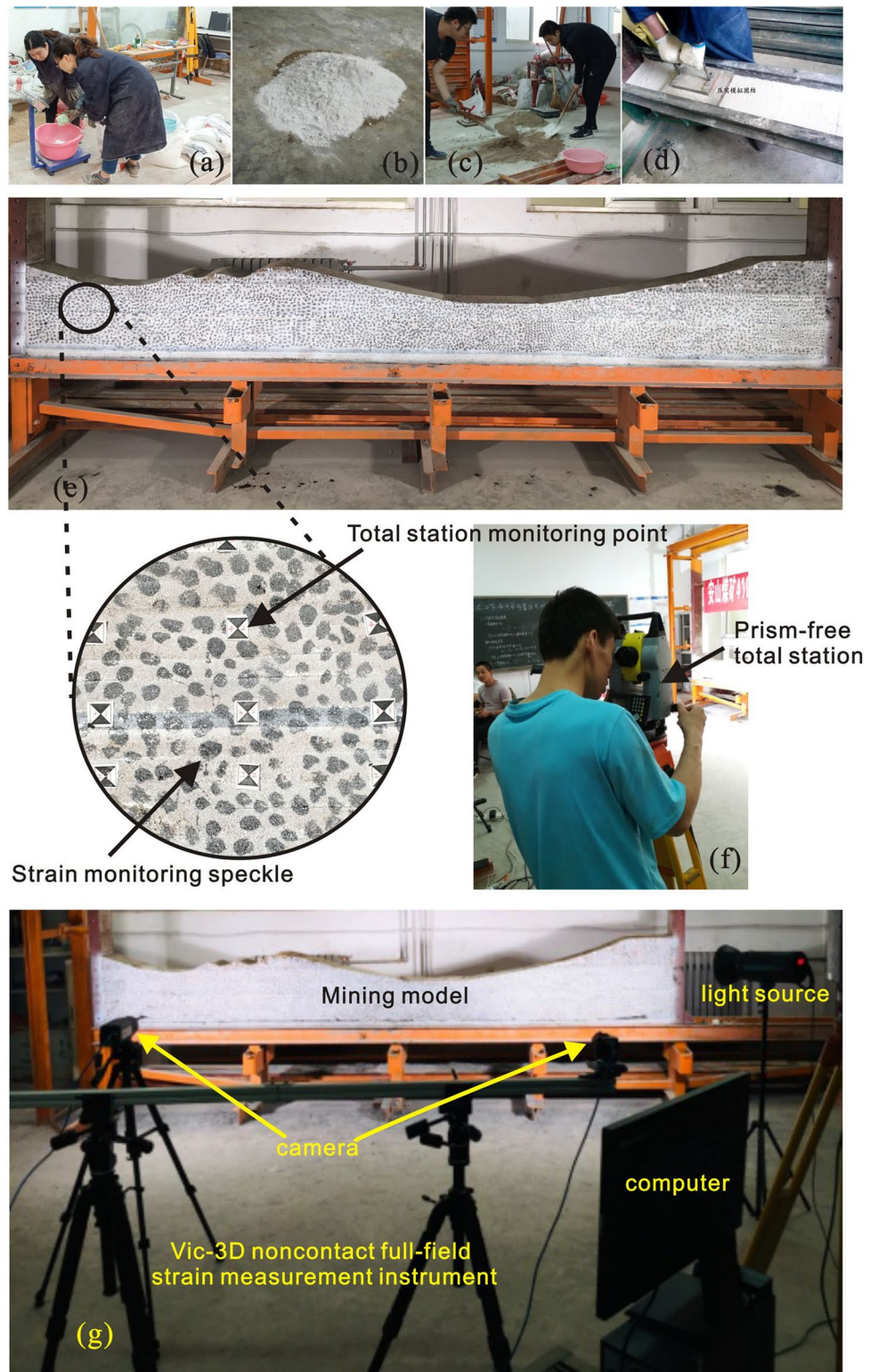
In order to improve the reliability of the coal mining model, it is necessary to establish a reasonable relationship between numerical parameters and macromechanical properties of rock mass (Potyondy and Cundall 2004). However, the Particle Flow Code (PFC) model makes use of the microstrength parameters of the rock mass, which has no direct mapping relationship with the macromechanical parameters of rock mass (Wang et al. 2014). These mesostrength parameters are usually determined through repetitive debugging of mechanical unit tests (uniaxial

Table 1 Microstrength parameters for numerical simulation (R_{min}, ball minimum radius [m]; R_{max}/R_{min}, ball size ratios; γ, bulk density [kg/m³]; E^*, ball effective modulus [GPa]; k_n/k_s, ball stiffness ratio; σ_t^*, flat joint tensile strength [MPa]; σ_c^*, flat joint cohesion [MPa]; f, micro-friction coefficient; β, moment-contribution factor; fa, internal friction angle [°])

Lithology	R_{min}	R_{max}/R_{min}	γ	E^*	k_n/k_s	σ_c^*	σ_t^*	β	f	fa
Loess layer	0.2	2.0	1702	0.24	2.0	0.165	0.055	0.4	0.4	20
Weathering bedrock	0.2	2.0	2200	6.3	2.0	12.0	4.0	0.3	0.25	25
Fine-grained sandstone	0.2	2.0	2780	10.0	2.0	17.1	6.7	0.1	0.5	50
Argillaceous siltstone	0.2	2.0	2760	6.7	2.0	15.9	5.3	0.5	0.5	27
Coal seam	0.2	2.0	1420	1.0	2.0	7.8	2.6	0.4	0.5	24
Siltstone	0.2	2.0	2760	7.0	2.0	16.2	5.4	0.2	0.5	30

compression test and Brazilian splitting test, etc.). Considering the complex shape and interlocking grain structure of minerals in real rock, it exhibits strong antirotation properties, as well as the compression-pull ratio characteristics of actual rock (the ratio of uniaxial compressive strength to tensile strength) (Wang et al. 2018). The linear parallel bond model, which is widely used in rock simulation, was employed in this work, and the moment contribution coefficient was incorporated, and mesostrength parameters of the numerical model were obtained through repeated debugging and calibration, as shown in Table 1. After calculation, the difference between the simulated macrostrength parameters and the actual macrostrength parameters of coal-rock mass (Table 2) is less than 5%, indicating that the microparameters in Table 1 are scientific and reliable and can be applied to the coal mining model illustrated in Fig. 5. The numerical model is built with the actual working face size of 1:1 in mind. The left and right sides and bottom of the model are fixed boundaries, while the top surface is constructed according to the geometry of the actual surface, which is a free boundary. The model's layered structure is determined by the actual stratigraphic sequence and lithology of the overburden, and an appropriate amount of random joints are set in each rock stratum to simulate pre-existing fractures. In order to meet the requirements of computation efficiency and

accuracy, the particle size is extended by a specific proportion (Song et al. 2020; Zhang et al. 2021). Once the rock mass strength parameters have been assigned, set the gravitational acceleration to 9.8 m/s² and compute the balance to complete the initial model building.

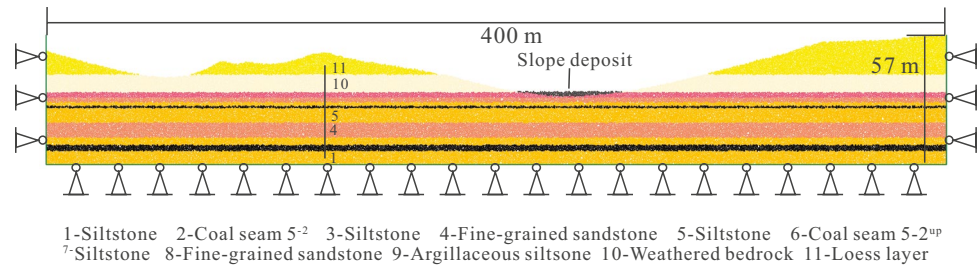## Result analysis

Overburden caving and fracture

In order to eliminate the boundary effect and ensure the stability of coal pillar, the left and right end of the model feature 20-cm coal pillars. Each excavation distance of the model is 10 cm. This research focuses on the characteristics and laws governing overburden and surface damage, omitting the temporary support effect of powered support in the working face. To comprehend the actual overburden damage, the experimental phenomena are presented in terms of the prototype's numerical values.

The overburden caving morphology and fracture development characteristics at different excavation stages are shown in Fig. 6. Comparing and analyzing the results of simulation test on similar materials with the findings of numerical simulations. When advancing to 50 m, the separation layer appeared, and the basic roof collapsed

Table 2 Comparison of the actual and numerical macroparameters

Lithology	Young's modulus E (GPa)			Uniaxial compressive strength σ_c (MPa)			Tensile strength σ_t (MPa)		
	Actual	Simulation	Error	Actual	Simulation	error	Actual	Simulation	error
Loess layer	0.4	0.4	0.00%	0.3	0.31	3.33%	0.035	0.036	2.86%
Weathering bedrock	10.0	10.1	1.00%	24.80	24.24	2.26%	2.68	2.66	0.75%
Fine-grained sandstone	17.0	17.3	1.76%	37.85	37.66	0.50%	3.88	3.85	0.77%
Argillaceous siltstone	11.0	11.5	4.55%	27.56	27.40	0.58%	3.35	3.33	0.60%
Coal seam	1.6	1.7	6.25%	14.65	14.48	1.16%	1.58	1.61	1.90%
Siltstone	12.3	12.1	1.63%	36.15	36.03	0.33%	3.62	3.67	1.38%

Fig. 5 Numerical model of particle flow in the Caigou section of the 125203 working face

1-Siltstone   2-Coal seam 5⁻²   3-Siltstone   4-Fine-grained sandstone   5-Siltstone   6-Coal seam 5-2ᵘᵖ
7-Siltstone   8-Fine-grained sandstone   9-Argillaceous siltsone   10-Weathered bedrock   11-Loess layer

for the first time (Fig. 6a, b). The length of the first collapse step in the physical simulation is about 36.5 m, and the cantilever beam structure is formed during this step (Fig. 6a). The numerical simulation generates upward developed vertical fractures above the open cut and working face, so that the initial collapse step of the numerical simulation is equal to the coal seam mining step, which is 50 m (Fig. 6b). The collapse characteristics of overburden obtained by the two test methods are very similar. As the advancing distance rose, the water-flowing cracks gradually developed upward, and the damage degree of the overburden gradually increased. The lower overburden collapsed and filled the goaf, while the upper overburden fracture formed an articulated masonry beam structure. When mining to a depth of 100 m, visible cracks occur on the surface (Fig. 6c, d).

The roof collapses periodically as the working face advances, and the surface fissures increase gradually in size. When mining to 210 m, the working face is just beneath the Caigou ditch. At this point, the 12th collapse occurs in the goaf, the caving body measures 194 m in length, the collapse angle on one side of the working face is 70°, and cracks emerge at the foot of the slope (Fig. 6e, f). It is completed when mining reaches 360 m, and fresh surface cracks form behind the working face (Fig. 6g, h). During the whole mining process, the rock formations were cut into blocks and showed periodic collapse; there are 15 surface cracks with an average step distance of 10 m; as the depth of the rock layer decreased, the fractures gradually became sparse and developed linearly. The results of simulation test on similar materials are fairly similar to those of numerical simulation. As a result, the reliability of the numerical model is established.

Figure 7 illustrates the real-time measurement results of the falling height and water flowing fracture zone height during mining. With staged coal seam mining, the overburden falls with a periodicitable pattern. Roof caving begins when the working face advances 43 m from the cut; this finding is quite similar to the field observation that the initial collapse step distance of the basic roof is 45.02 m. During subsequent mining, the average periodic caving step distance is 10 m. Throughout the period of coal seam mining to a depth of 95 m, the overburden falling height gradually grows to 6 m, and the surface settlement reaches a maximum of 16 cm.

Subsequently, when the mining advance distance increases, the overburden height and mining distance stabilize.

The development height of the water-flowing fractured zone is 4 m at the initial pressure. When the working face reaches 60 m, the development height of the overlying rock water-flowing fracture zone increases to 17 m and remains stable. Until the working face reaches 109 m, with the periodic roof falling, the height of the water-flowing fracture zone changes again and becomes directly connected to the surface, forming surface fractures. When the working face passes through Caigou, the surface cracks on the slope are relatively developed, while the upward cracks in the goaf are preferentially connected.

The macrocrack in the rock mass is the consequence of tens of thousands of microfractures extending and expanding in space. Microfractures grow, extend, and accumulate to form macrocracks. When it vertically penetrates the rock stratum, the rock stratum breaks. As can be observed, the macroscopic failure of rock strata is the accumulation of mesodamage, which is manifested in the dynamic evolution process of "microfracture generation–microfracture expansion and extension–microfracture collection and penetration–rock stratum failure." Therefore, analyzing the evolution law of microfractures is critical for the formation of macrocracks. As illustrated in Fig. 8, the variation curve of the number of microfractures with the mining distance presents two stages: the first stage occurs when the mining distance is less than 100 m, at which point the number of fractures increases exponentially with the mining distance. The second stage is when the mining distance exceeds 100 m, the number of fractures increases linearly with the mining distance. Each step has the following curve formula:

$$N = \begin{cases} 151 * 1.03^{\wedge}L & (L < 100) \\ 30.78 * L + 273 & (L \geq 100) \end{cases}$$

(1)

When the stress between overburden particles exceeds their ultimate strength as a result of deformation accumulation, the bonding between particles is destroyed and microcracks occur. Therefore, the damage degree of overburden can be quantitatively analyzed by the number of
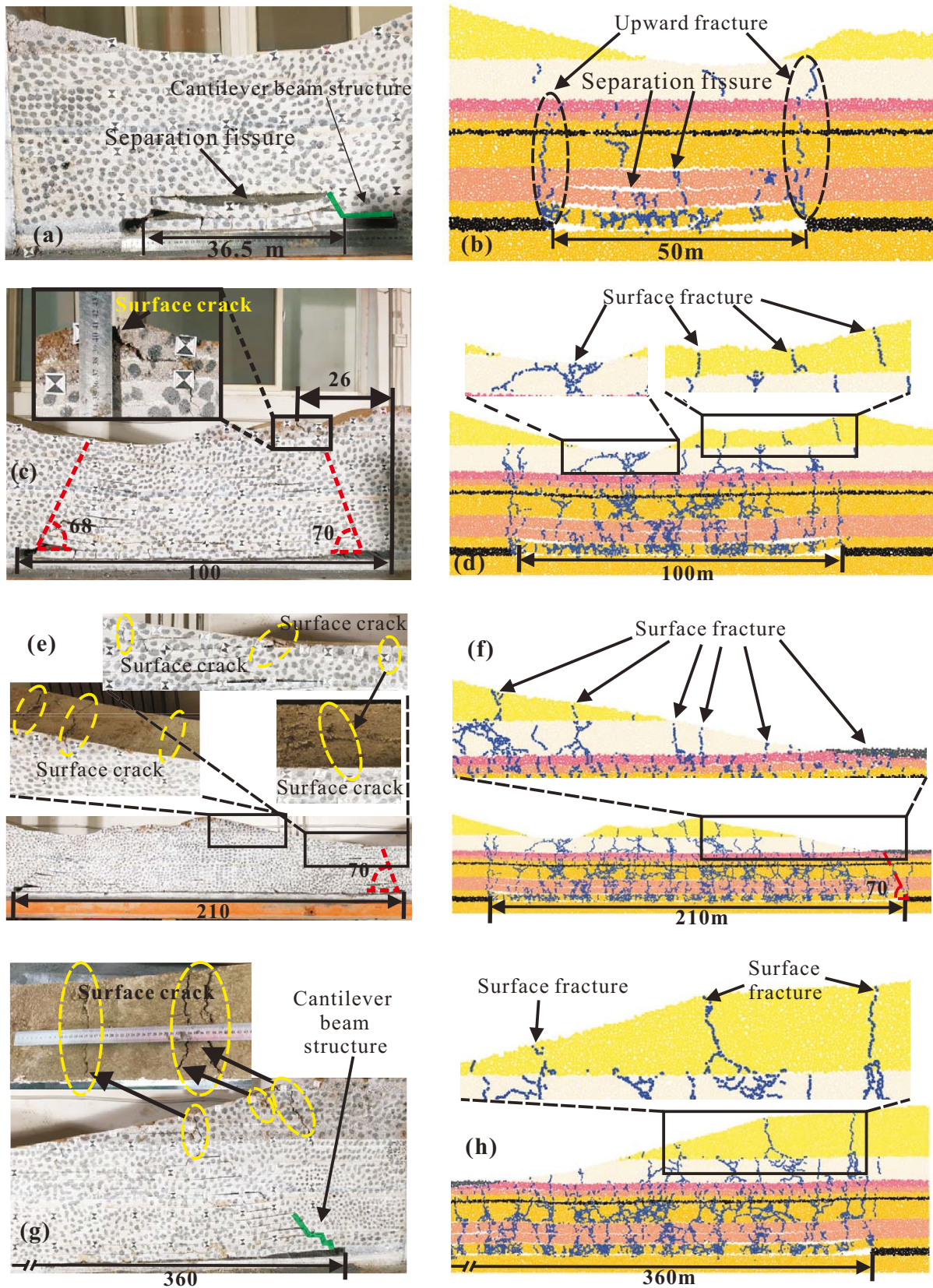
Fig. 6 Characteristics of overburden failure and fracture development in Goaf. Among them, (**a**), (**c**), (**e**), and (**g**) are the simulation results of similar materials; (**b**), (**d**), (**f**), and (**h**) are numerical simulation results
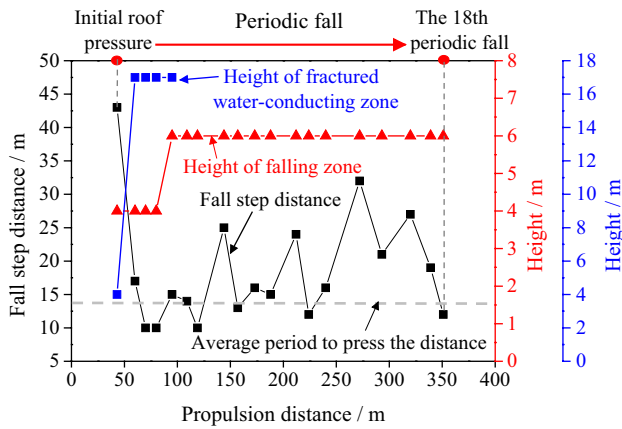
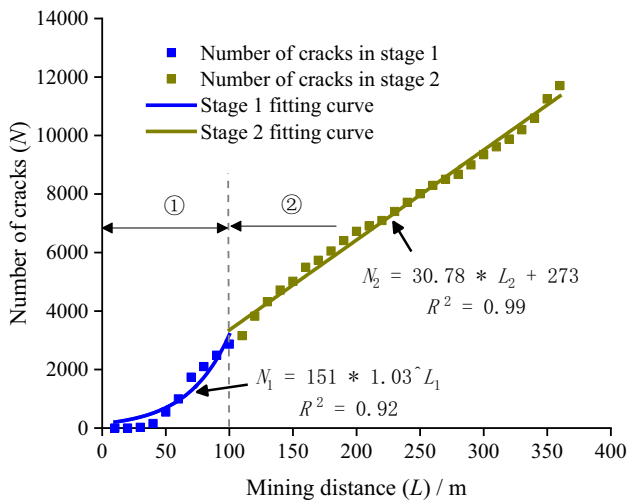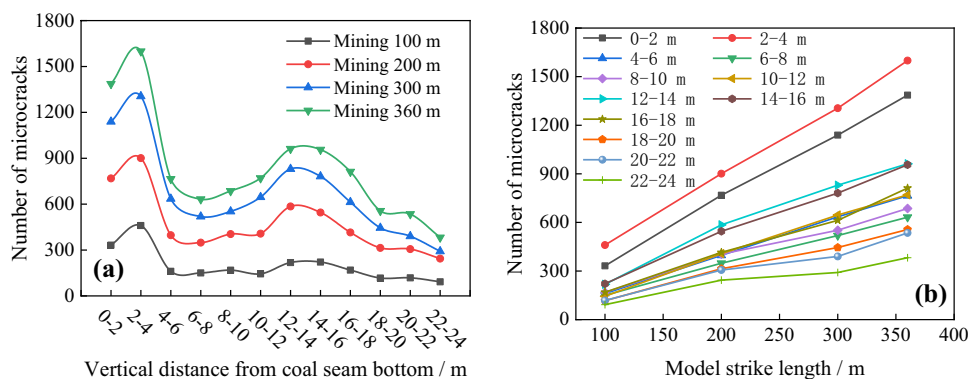**Fig. 7** Characteristics of overburden collapse and the law of the fractured water-conducting zone

Fig. 8 Variation curve of fracture number with mining distance in numerical simulation

microfractures in various layers and advancing distances. It can be seen from Fig. 9a, the number of microcracks generated by overburden failure as a function of overburden

height (taking the bottom of the coal seam as the datum plane) exhibits bimodal curve characteristics at various mining distances. The number of microcracks reaches a phased peak in the range of $2 \sim 4$ m and $12 \sim 16$ m, respectively, and the value of the second peak is about 0.6 times that of the first. Comparison from the perspective of lithology, it is revealed that between 4 and 12 m, fine-grained sandstone with high strength, resulting in few microfractures caused by its failure. At the upper part, there is siltstone with low strength, which increases the number of microcracks. Then, the closer to the surface, the less cracks there are. Figure 9b shows that the number of microcracks in each layer increases linearly with the advance of the working face. It demonstrates that the amount of microfractures in the rock stratum is basically identical under the same excavation footage.

## Vertical deformation monitoring of overburden

Figure 10 shows the VIC-3D imaging and numerical simulation vertical displacement nephogram of overburden rock vertical deformation after coal mining. Two methods produce remarkably comparable results. When combined with the comparative analysis in Fig. 6, with the continuous advancement of the coal mining face, the overburden area with significant vertical deformation gradually overlaps the failure range of the overburden. The vertical deformation of the overburden continuously evolves to the surface, and the vertical subsidence increases with depth. During excavation, there is a vertical deformation concentration area in the center of the direct roof. When excavation depth reaches 100 m, there are two deformation concentration areas in the roof, the vertical deformation contour shows "M-type" characteristics, and the surface vertical deformation changes dramatically, the surface subsidence value reaches 1.6 m, and the full mining state is achieved. When excavation reaches a depth of 210 m, obvious deformation develops along the consequent slope. When excavation reaches 360 m, it passes through Caigou completely. As a result of the periodic caving of the overburden and topography, the vertical deformation contour of overburden shows wavy characteristics.

Fig. 9 Statistics of number of microfractures. (**a**) Variation curve of number of microfractures with height; (**b**) variation curve of microfracture number with mining distance

Fig. 10 Vertical deformation characteristics of overburden. (**a**) Simulation results of similar materials. (**b**) Numerical simulation results
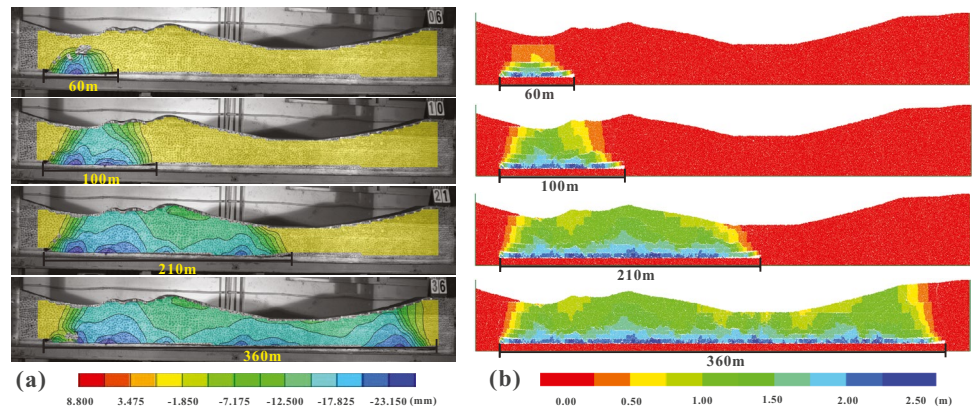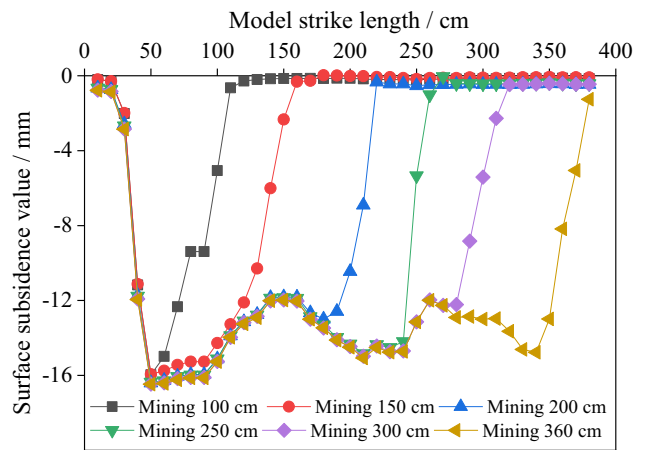

According to the vertical displacement curves of each monitoring layer following coal mining (Fig. 11a), the vertical displacement of the ov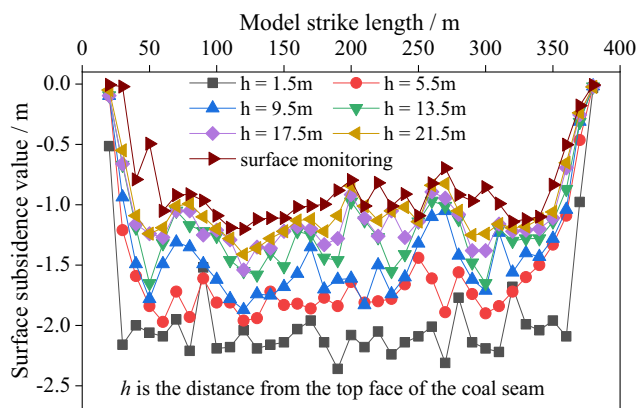erburden is basically symmetrical as the center Caigou Valley, and it exhibits the "M-type" vertical displacement variation characteristics in the main gully section of Caigou. The vertical displacement of the
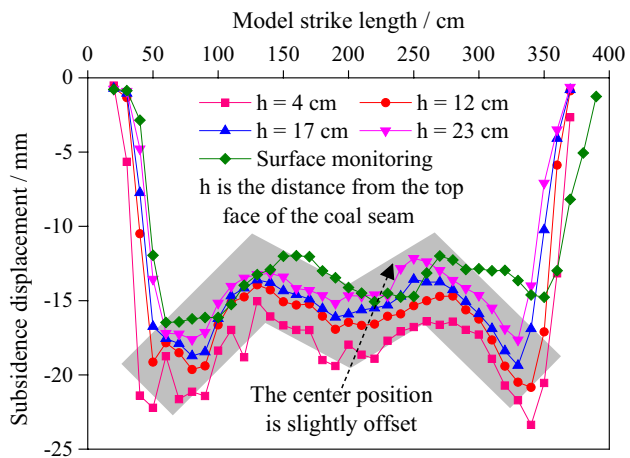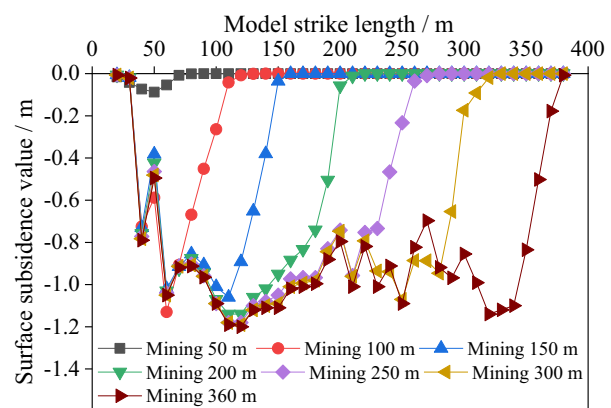

Fig. 11 Vertical displacement monitoring curve of overburden. (**a**) Vertical displacement curves of different layers in similar material experiments; (**b**) Surface vertical displacement curves of in the different mining stages of similar material experiments; (**c**) Vertical dis-placement curves of different layers in numerical simulation experiments; (**d**) Surface vertical displacement curves of in the different mining stages of numerical simulation experiments

gully position is large, and the vertical displacement trend towards the two sides of the slope varies. At the same time, when the monitoring point approaches the surface, the center of the vertical displacement curve shifts slightly to the working face, and the vertical displacement change trend of the overburden is significantly affected by the topography. The maximum subsidence of the Caigou ditch bottom is approximately 1.5 m, and that of the slope shoulder is approximately 1.2 m. The surface subsidence curve during coal mining is depicted in Fig. 11b. When the coal seam is mined to 100 m, the mining process reaches the full mining degree, and the surface subsidence reaches the maximum value (1.6 m). This is consistent with the results of microfracture analysis. The numerical simulation results closely match the simulation test results of similar materials in terms of the overburden deformation and surface subsidence rules and characteristics (Fig. 11c, d), with the surface subsidence showing "M"-type features. The maximum surface subsidence of the numerical model is 1.2 m; the numerical model produces more errors than the simulation test of similar materials. This is because the particle size of the numerical model is larger than the actual particle size.

A comprehensive analysis demonstrates that overburden deformation evolves and renews continually during the coal seams mining process. When strain accumulation reaches its deformation limit, the overburden collapses, and the rock settlement deformation increases, resulting in separation cracks, rock fracture cracks, and surface cracks. When the span of the goaf gradually increases to a specific range, the overburden cracks connect with the surface cracks, forming water-conducting cracks that develop at the surface. Moreover, when the coal seam is mined 100 m, mining reaches the full mining state. After passing through the bottom of the Caigou ditch, the ditch bottom reaches a maximum subsidence value of 1.5 m. After the ecssation of coal mining, surface subsidence takes on a "M" shape.

Fragmentation and fragment size

Figure 14 depicts numerical simulations of the fragmentation process during the overburden collapse (The color in the figure represents the random ID number of fragments, which has no physical meaning). During the overburden collapse stage, the fragment size (fragment length) of each rock stratum gradually increases from the low- to high-level position. With the continuous advancement of the working face, the fragment size of early stage overburden collapse is large (Fig. 12a, b). Later on, as the overburden continues to collapse, the larger fragments preceding the low-level position are impacted into small fragments (Fig. 12c–e). When mining completed, the change in fragment size within each rock stratum is minimal (Fig. 12f, g). The size statistics of fragments indicate the degree of rock fragmentation (Gao et al. 2020b). As displayed in Fig. 13, the majority of fragment sizes fall within the range of 0.2~3.5 m, and the quantity of fragments of various sizes is described by a power exponential function. The fragment size ranges between 0.2 and 5 m, and the number of fragments shows a rapid decrease with increasing fragment size, followed by a show decrease (> 5 m). With the rising collapse position of overburden, larger fragments
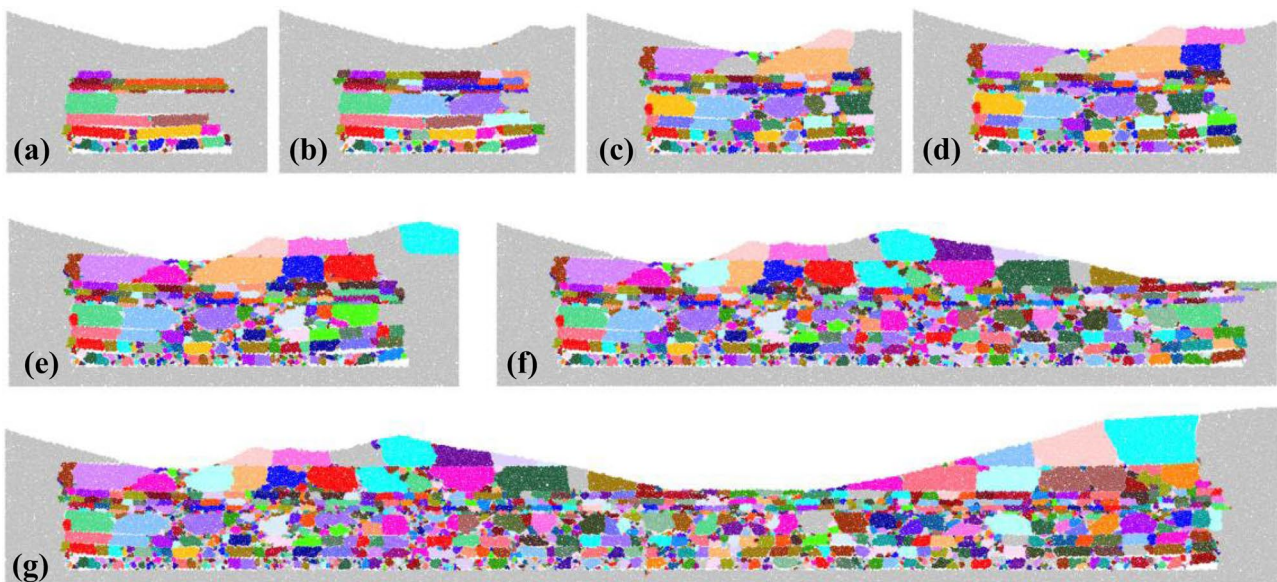
Fig. 12 Evolution of overburden collapse fragments: (**a**) mining 50 m; (**b**) mining 60 m; (**c**) mining 70 m; (**d**) mining 80 m; (**e**) mining 100 m; (**f**) mining 210 m; and (**g**) mining 360 m

$$N = 8 + 1201 * e^{(-L/1.3)}$$
$$R^2 = 0.99$$
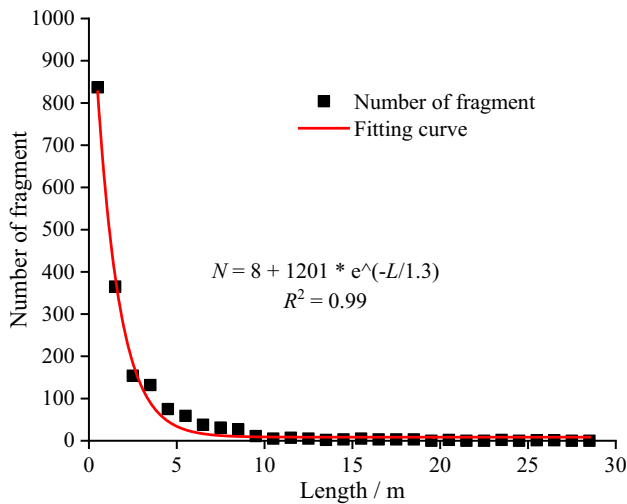
Fig. 13 Number distribution of fragments of different sizes when mining 360 m

at the lower layer are gradually broken down into small-size fragments, resulting in an increasing number of small-size fragments and a diminishing of large-size fragments. Most large fragments are distributed near the surface, while small fragments are concentrated in the collapse zone (Fig. 14).

Force chain evolution

Force chain has certain structural characteristics, which have common physical facts with the basic concept of skeleton in macromechanics (Wang et al. 2020b). Therefore, the evolution of the force chain grid can be analyzed by the mechanical properties of the particle system. After the rock mass is shattered, the accumulation body can be regarded as a huge
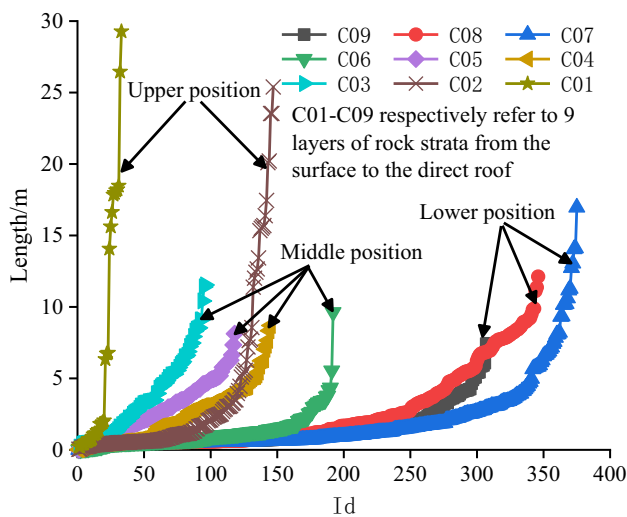

Fig. 14 Fragment size distribution in different horizons

volume of loose rock block. Therefore, the characteristics of the strong chain (contact force greater than average contact force) between blocks can reflect the macromechanical characteristics of rock blocks.

In the process of coal mining, the evolution law of the force chain in the discontinuous structure system of overburden rock is critical for determining the degree of overburden damage and the development height of water-flowing fissures, especially for the formation of the strong chain arch and the supporting effect of the strong chain on the overburden rock.

The excavation of the coal seam breaks the initial equilibrium state of the force chain, and the force chain of the surrounding rock redistributes to find a new equilibrium state automatically (Fig. 15). From the coal wall to the deep part of the rock mass, there are apparent strong force chain areas and original force chains (distribution state of the force chain under the action of the original rock stress). The strong force chain area is the primary bearing area of the whole surrounding rock, and the weight of the overlying rock mass is transferred to the strong chain area via the path and direction of the force chain. However, mining has had a negligible effect on the deep original force chain area, which is essentially in its original rock stress state. In the initial excavation stage, when the force chain around the stope deflects due to the difference in the layered structure of the overburden rock, a vertically alternating layered composite force chain arch of "strong–weak–strong–weak" forms. Both ends of the stope have obvious stress concentrations, and the strong force chain is mostly compressive stress, and the tensile stress of low strength occurs between the strong chains. A strong force chain arch surrounds the entire goaf overburden. The formation of a strong force chain arch is the result of the surrounding rock stress self-organization. The strong force chain area is the bearing capacity system of the surrounding rock that maintains stability and prevents further damage (Fig. 15a–c). The working face advances forward as the overburden collapses and the goaf fills. The strength chain in the middle of the model is not a large-scale force chain arch that alternates up and down in the initial stage, but rather a series of "M-type" continuous small force chain arches, and "triangle" force chain arches with large spans are produced at the open cut and working face location (Fig. 15d–g). When combined with the distribution characteristics of overlying rock fractures in the goaf, Fig. 6 demonstrates that the arch foot strength chain basically coincides with the rock mass fracture position, whereas the arch top strength chain mainly refers to the upper surface position of the broken rock block, which is also the upper surface of the masonry beam structure.

The measurement indicates that the average span of the arch foot of the middle small-sized strong chain arch is 10 m, which is roughly equal to the periodic collapse step of the overburden. At both ends of the cut off and working face, the "triangular" force chain arch spans approximately
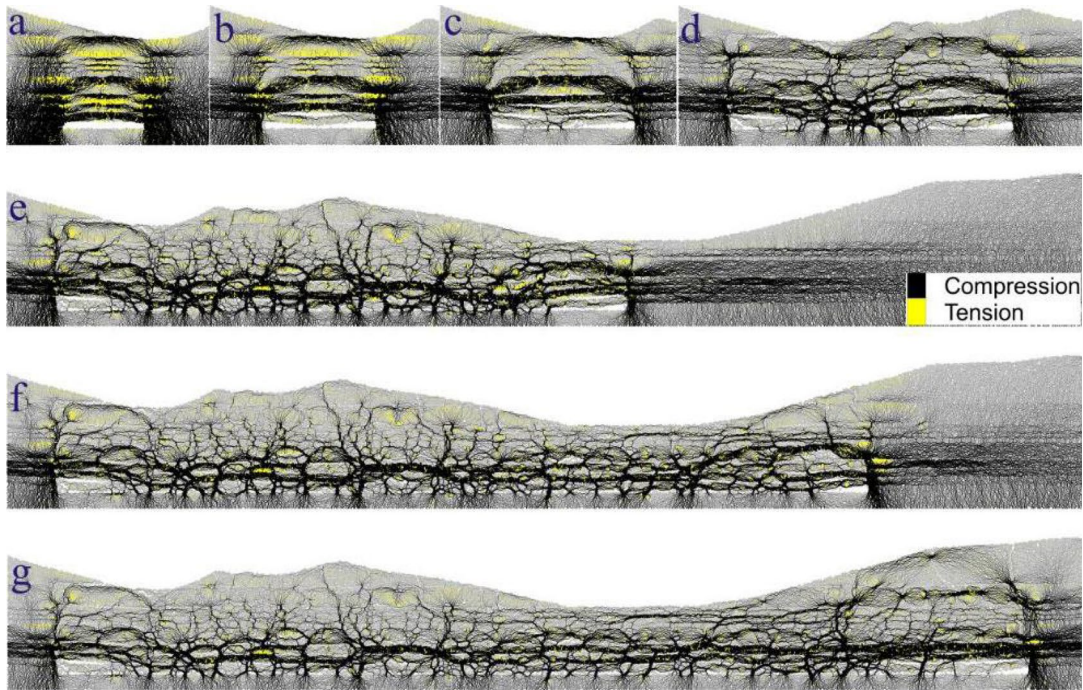
Fig. 15 Force chain evolution in different mining stages: (**a**) mining 30 m; (**b**) mining 40 m; (**c**) mining 50 m; (**d**) mining 100 m; (**e**) mining 210 m; (**f**) mining 300 m; and (**g**) mining 360 m

30 m and 40 m, respectively. Continuous advancement of the working face is accompanied by periodic crushing, collapse, and overburden accumulation in the goaf. At the compaction position of the broken rock blocks on both sides of the collapsed body and at the position of the collapsed rock mass's upper surface, the force chain is relatively long. Together, they form a strong chain arch. These powerful chain arches support the overburden to a certain extent, bear the main load of the overburden, and serve as the bearing capacity system of the backbone. Between the strong chains, the weak oblique force chains can maintain and enhance the stability of the surrounding strong chains. This force chain accurately depicts the discontinuous and incompatible deformation characteristics of overburden caused by the strength difference between the rock strata and the accumulation characteristics of fault rock blocks, in contrast to the continuous deformation and continuous gradient stress arch characteristics obtained by the finite element method (FEM) and finite difference method (FDM) simulation.

The main bearing structure is the strong force chain, and the percentage of strong force chain in the total contact force can reflect the damage characteristics of overburden to a certain extent. Therefore, we introduce a new notion called the strong chain coefficient, which refers to the ratio of strong force chains to total force chains in number. Figure 16 indicates the strong chain coefficients at various stages of mining. As can be seen,

the strong chain coefficient shows a negative tendency when the mining distance is less than 100 m; when the mining distance is greater than 100 m, the strong chain coefficient varies between 0.27 and 0.31 with an average value of 0.29. It demonstrates that, prior to full mining, the proportion of strong chain drops progressively as the mining distance increases; after full mining, the proportion of strong chain is less affected by mining.
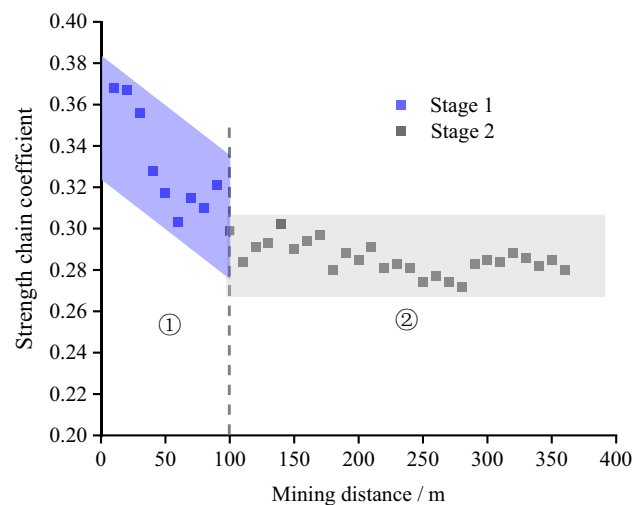
Fig. 16 Variation characteristics of strength chain coefficient

Height of caving zone

A comprehensive comparative analysis of the vertical displacement, fracture, fragmentation, and force chain properties of the overburden in the goaf is shown in Fig. 17. The overburden damage features are basically consistent in the area with a strong force chain, the area with a high degree of fragmentation, the area with densely developed fractures, and the area with a strong vertical displacement of the roof, with a caving zone height of 9.9 m. Figure 17c reveals that the fracture degree of the overburden layer gradually decreases from bottom to top, showing that the size of the rock block (fragment width) is small in the lower part and gradually increases in the upper part, which is generally consistent with the actual fracture characteristics of the overburden layer. In addition, Fig. 17b and d demonstrate that the arch foot position of the strength force chain coincides with the densely developed fault zone.

Fig. 18 Measured development height of the caved zone

Discussion

The key parameter to prevent roof water disasters, gas outbursts, and other mine disasters is the development height of water-flowing fissures in the overburden. The comprehensive comparison of field investigations, similar material simulations, and numerical simulations illustrates that the development height of mining-induced water flow fracture zones is greater than the thickness of the overlying rock and soil layer, especially the trench bottom position, indicating that the water 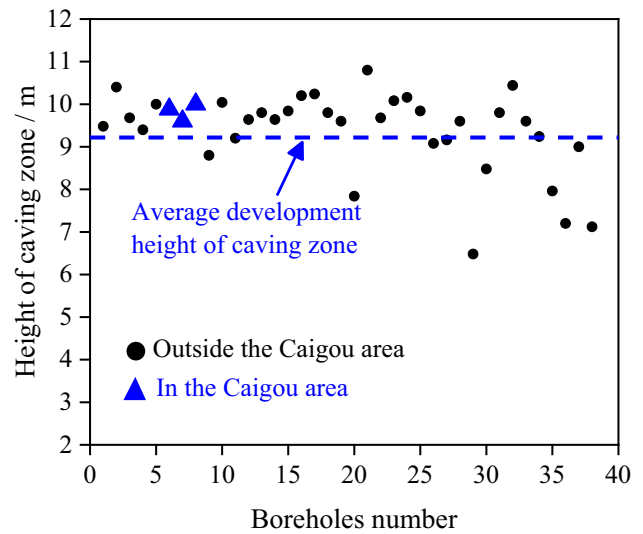flow fracture develops directly to the surface and forms surface cracks. According to the analysis of 38 groups of field drilling data in the Anshan coal mine area (Fig. 18), the maximum, minimum, and average development heights of the caved zone are 10.8 m, 6.48 m, and 9.23 m, respectively. The boreholes in the Caigou area are No. 6, No. 7, and No. 8, with corresponding measured caved zone heights of 9.88 m, 9.6 m, and 10.0 m, respectively, with an average of 9.83 m.

The development height of the caving zone is compared and analyzed using on site measurements, similar material
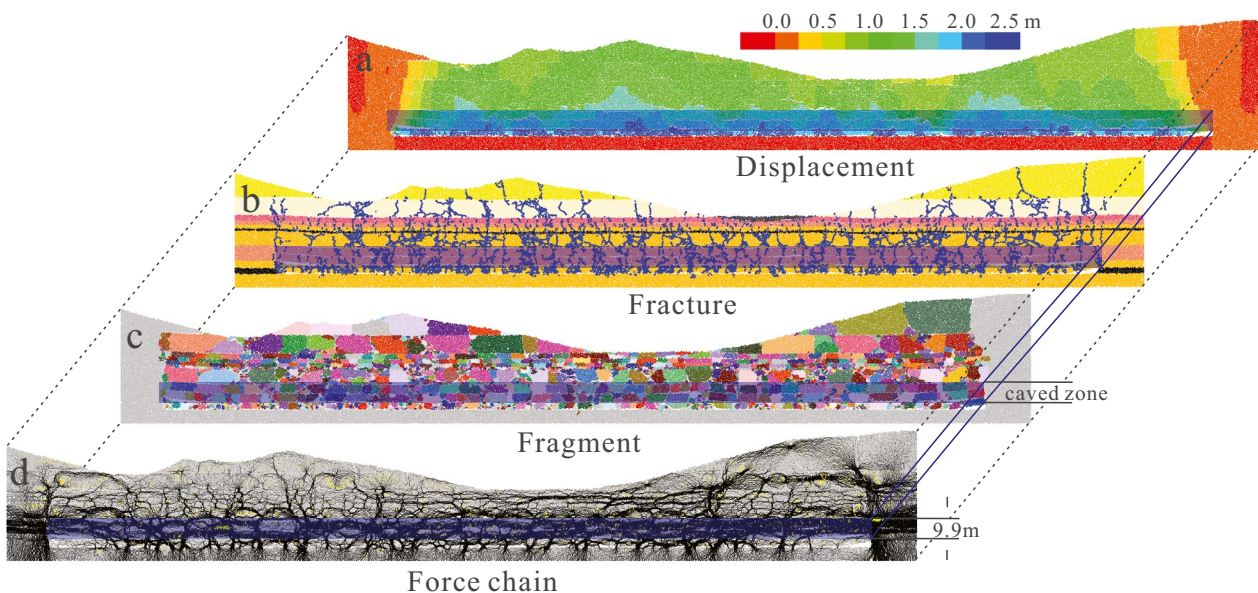

Fig. 17 Comprehensive analysis of the caved zone after mining. (**a**) Vertical displacement diagram. (**b**) Fracture distribution map. (**c**) Fragment diagram. (**d**) Force chain distribution diagram

Table 3 Comparison of the development height of the caved zone by different methods

| Research methods	Similar material experiment	Numerical simulation	Measured average value
Height value (m)	6	9.9	9.83

simulation tests, and numerical simulations (Table 3). The height of the collapsed area produced through numerical simulation is extremely close to the height obtained through field measurements, while the height obtained by the similar material experiment is less than the height from field measurements. The analysis proves that similar material experiments monitor the caved zone height by interpreting the macroscopic deformation characteristics of the overburden obtained through visual observation by experimenters, which has some subjectivity and conservatism, resulting in a relatively small result. However, since the numerical simulation results are integrated with a range of characteristic indexes through comprehensive judgment and analysis, they are extremely close to the measured results. Simultaneously, the fracture development laws of the overburden obtained by the two simulation methods are strongly comparable, exhibiting the features of "two zones," and are basically consistent with the actual situation. As a result, it can be concluded that the overlying rock water-flowing fracture zone may be directly connected to the surface after trench mining in the Caigou coal mine, and the caved zone is approximately 9.83~9.9 m in height. Accurate judgment and measurement of the collapse zone height have certain guiding significance for the prevention and control of surface cracks and water burst disasters.

The discontinuous deformation and failure results of overburden such as separation fracture development, rock fracture, and collapse simulated in this paper are basically consistent with the numerical simulation results of Yang et al. (2011), Gao et al. (2014), and Ju et al. (2019) using RFPA, UDEC, and CDEM, respectively, and the evolution process of overburden strong chain arch formation, expansion, and failure before full mining is consistent with the simulation results of Zhang et al. (2021), indicating that the research findings in this paper are credible. However, when topography and overburden discontinuous deformation are considered, the

overburden and surface subsidence display wavy variation laws and "M" type subsidence curve attributes, which differ from the inverted single peak characteristics without considering the influence of topography (Liu et al. 2019a, b; sun et al. 2019). At the same time, the characteristics of a small "m" strong chain arch with a backward continuous distribution of overburden span in shallow coal seam mining obtained in this study are distinct from the continuous stress distribution and single stress arch features of overburden roof simulated by numerous experts using FEM and FDM (Meng et al. 2016; Zhang et al. 2019; Xing and Han 2020), as well as the single stress arch characteristics of deep coal seam roof considered by Kang et al. (2018) (Fig. 19). Therefore, for the study of overburden deformation and stress characteristics following shallow coal seam mining, the research method in this paper can accurately reflect the discontinuous and uncoordinated deformation law and stress distribution characteristics of each rock stratum due to their physical differences.

When the distribution characteristics of microfractures and fractured rock blocks are combined, it is clear that during initial mining, the stress of the surrounding rock is redistributed, the stress of the overburden roof is released, and the overburden load is transmitted to the surrounding rock near coal pillars on both sides along the deflected force chain, forming a strong chain area, and forming a strong chain arch with the strong chain on the upper surface of roof rock layer to support the load on the arch. When the stress at the position of the strong chain exceeds the bond strength between particles, the bond is destroyed, the force chain becomes unstable, and microcracks form. Then, the stress is concentrated and gradually released around the microcracks, the strong chain is constantly renewed and destroyed, and the microcracks are continuously extended and expanded, eventually grouping together to form macrocracks. When a macrocrack penetrates a rock stratum, the rock stratum breaks and collapses. Due to the continuous evolution of the strong chain arch to the near surface, the cracks continue to develop upward until they penetrate the surface and form surface cracks. With the periodic collapse of overburden, the particles on both sides of the rock block are squeezed to form a small M-shaped strong chain. This strong chain is composed of a strong contact force chain with the upper surface of the rock block, forming a new strong chain support structure. Therefore, it can be found that the arch foot strength chain roughly coincides with the position of rock fracture. Thus, the force

Fig. 19 Stress distribution characteristics of overburden after coal seam mining. Left: shallow buried trench mining; Right: deep seam mining

■ Coal seam   ↓↓↓ Overburden pressure   ⌒ Strong force chain arch
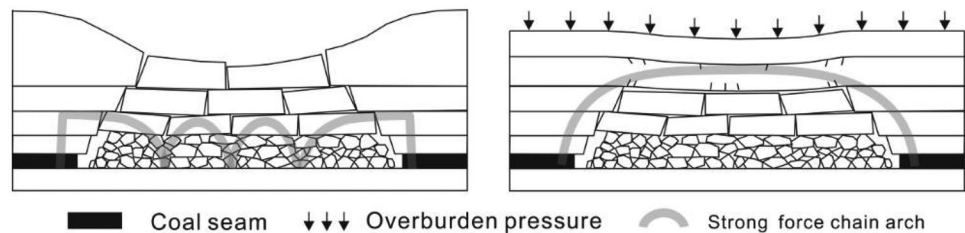
chain evolution between particles can accurately reflect the discontinuous damage characteristics of overburden caused by the strength difference between strata and can reveal the failure mechanism of mining overburden from the mesoscale.

A comprehensive comparison of the field surface fracture characteristics with similar material experiments and numerical simulations of the overburden damage characteristics reveals that the three methods produce essentially consistent results, elucidating the overburden damage mechanism during mining beneath the channel of a shallow coal seam. When the coal seam is mined, the stress of the surrounding rock redistributes, and constant deformation of the rock stratum accumulates. When the deformation approaches its limit, the overlying rock periodically breaks and caves, and upward water-flowing fractures develop. When fractures reach the surface, surface cracks emerge. Landslides occur in the slope region as a result of the damage caused by surface cracks and the gravity of rock and soil mass, and the ditch bottom collapses. Additionally, during periods of heavy rainfall, gully surface cracks can readily become surface rivers, resulting in mine water disasters.

Conclusion

In this paper, the development law of surface cracks on site is investigated and analyzed, and the laws of overburden failure, fracture evolution, force chain evolution, and fragment distribution are simulated. The development height of the overburden caving zone and water-flowing fracture zone caused by coal mining is analyzed and discussed in conjunction with actual borehole data. The conclusions are as follows:

1. Through the remote sensing interpretation of UAVs and field surveys, surface cracks are mostly linear "step cracks" parallel to the direction of the opening cut. The overburden deforms as the working face advances, and the strength difference and uncoordinated deformation between strata lead to separation cracks between strata, and the overburden has the cyclic deformation and "separation of strata–caved and disappearance of separation–generation of high-level separation" damage. The periodic caving step distance is 10 m, the caving zone height is 6 m, and the water-flowing fractures develop directly to the surface cracks.

2. Due to the influence of topography and periodic caving of the overburden, the vertical subsidence curve of the overburden essentially presents a symmetrical "M"-type variation characteristic with the valley as the center. When the coal seam is mined to 100 m, it reaches the full mining stage. When combined with the results of VIC-3D imaging, the vertical deformation contour of the overburden shows wavy characteristics.

3. As burial depth decreases, the cracks in the overburden rock gradually diminish and transition from a banded aggregation state to a linear feature, and the number of microfractures increases with the mining distance presenting two stages. The overburden and surface deformation characteristics are largely compatible with the experimental results. The height of the caved zone is 9.9 m, due to the caving characteristics, fracture development, vertical displacement, fragment characteristics, and force chain arches.

4. The degree of overburden fragmentation grows gradually from top to bottom. At the initial stage of excavation, the force chain exhibits the features of a "strong–weak" alternating composite force chain arch. The periodic caving stage shows the characteristics of multiple "M"-type adjacent small-sized strong chain arches. The position of the arch foot of the strong chain corresponds to the position of the water-flowing crack, and the average span of the arch foot is 10 m. The fragment size of each rock stratum is characterized by the gradual increase from the low-level position to the high-level position.

Author contribution Jiangbo Wei: methodology, software, data curation, writing–original draft, experiment. Shuangming Wang: conceptualization, methodology, writing–review and editing. Shijie Song: methodology, writing–review and editing. Qiang Sun: writing–review and editing. Tian Yang: investigation, validation, experiment.

Declarations

Conflict of interest The authors declare no competing interests.

References

Bai E, Guo W, Tan Y (2019) Negative externalities of high-intensity mining and disaster prevention technology in China. Bull Eng Geol Environt 78(7):5219–5235

Bai Q, Tu S, Wang F, Zhang C (2017) Field and numerical investigations of gateroad system failure induced by hard roofs in a longwall top coal caving face. Int J Coal Geol 173:176–199

Behera B, Yadav A, Singh G, Sharma S (2019) Numerical modeling study of the geo-mechanical response of strata in longwall operations with particular reference to Indian geo-mining conditions. Rock Mech Rock Eng 53(4):1827–1856

Cao W, Shi JQ, Si G, Durucan S, Korre A (2018) Numerical modelling of microseismicity associated with longwall coal mining. Int J Coal Geol 193:30–45

Gao F, Kang H, Lou J, Li J, Wang X (2019) Evolution of local mine stiffness with mining process: insight from physical and numerical modeling. Rock Mech Rock Eng 52(10):3947–3958

Gao F, Stead D, Kang H, Wu Y (2014) Discrete element modelling of deformation and damage of a roadway driven along an unstable goaf-a case study. Int J Coal Geol 127:100–110

Gao G, Meguid MA, Chouinard LE (2020a) On the role of pre-existing discontinuities on the micromechanical behavior of confined rock samples: a numerical study. Acta Geotech 15(12):3483–3510

Gao G, Meguid M, Chouinard L, Xu C (2020b) Insights into the transport and fragmentation characteristics of earthquake-induced rock avalanche: numerical study. Int J Geomech 20(9):04020157

Ghabraie B, Ren G, Zhang X, Smith J (2015) Physical modelling of subsidence from sequential extraction of partially overlap ping longwall panels and study of substrata movement characteristics. Int J Coal Geol 140:71–83

Guo W, Zhao G, Bai E, Guo M, Wang Y (2021) Effect of overburden bending deformation and alluvium mechanical parameters on surface subsidence due to longwall mining. Bull Eng Geol Environt 80(3):2751–2764

Guo W, Zhao G, Lou G, Wang S (2018) A new method of predicting the height of the fractured water-conducting zone due to high-intensity longwall coal mining in China. Rock Mech Rock Eng 52(8):2789–2802

Guo W, Zhao G, Lou G, Wang S (2019) Height of fractured zone inside overlying strata under high-intensity mining in china. Int J Rock Mech Min Sci 29:45–49

Jiang Z, Lei S, Cao H, Guo L, Zhang J, Qiao X (2017) Coal mining under river recharged by desert. J China Coal Soc 42(1):73–79

Ju Y, Wang Y, Su C, Zhang D, Ren Z (2019) Numerical analysis of the dynamic evolution of mining-induced stresses and fractures in multilayered rock strata using continuum-based discrete element methods. Int J Rock Mech Min Sci 113:191–210

Kang H, Lou J, Gao F, Yang J, Li J (2018) A physical and numerical investigation of sudden massive roof collapse during longwall coal retreat mining. Int J Coal Geol 188:25–36

Kong DZ, Cheng ZB, Zheng SS (2019) Study on the failure mechanism and stability control measures in a large-cutting-height coal mining face with a deep-buried seam. Bull Eng Geol Environt 78(8):6143–6157

Liu C, Li H, Mitri H (2018) Effect of strata conditions on shield pressure and surface subsidence at a longwall top coal caving working face. Rock Mech Rock Eng 52(5):1523–1537

Liu H, Deng K, Zhu X, Jiang C (2019a) Effects of mining speed on the developmental features of mining-induced ground fissures. Bull Eng Geol Environt 78(8):6297–6309

Liu Z, Zhong X, Botao Q, Ren H, Gao A (2019b) Redevelopment of fractures and permeability changes after multi-seam mining of shallow closely spaced coal seams. Arch Min Sci 64(4):671–686

Majdi A, Hassani FP, Nasiri MY (2012) Prediction of the height of destressed zone above the mined panel roof in longwall coal mining. Int J Coal Geol 98:62–72

Meng Z, Shi X, Li G (2016) Deformation, failure and permeability of coal-bearing strata during longwall mining. Eng Geol 208:69–80

Mondal D, Roy P, Kumar M (2020) Monitoring the strata behavior in the Destressed Zone of a shallow Indian longwall panel with hard sandstone cover using Mine-Microseismicity and Borehole Televiewer data. Eng Geol 271:105593

Potyondy D, Cundall P (2004) A bonded-particle model for rock. Int J Rock Mech Min Sci 41(8):1329–1364

Rezaei M (2018) Development of an intelligent model to estimate the height of caving-fracturing zone over the longwall gobs. Neural Comput Appl 30:2145–2158

Rezaei M, Hossaini MF, Majdi A (2015a) A time-independent energy model to determine the height of destressed zone above the mined panel in longwall coal mining. Tunn Undergr Sp Tech 47:81–92

Rezaei M, Hossaini MF, Majdi A (2015b) Determination of longwall mining-induced stress using the strain energy method. Rock Mech Rock Eng 48(6):2421–2433

Song Z, Konietzky H, Herbst M (2020) Drawing mechanism of fractured top coal in longwall top coal caving. Int J Rock Mech Min Sci 130(6):104329

Sun Y, Zuo J, Karakus M, Wang J (2019) Investigation of movement and damage of integral overburden during shallow coal seam mining. Int J Rock Mech Min Sci 117:63–75

Tang J, Dai Z, Wang Y, Zhang L (2019) Fracture failure of consequent bedding rock slopes after underground mining in mountainous area. Rock Mech Rock Eng 52(8):2853–2870

Wang C, Zhang C, Zhao X, Liao L, Zhang S (2018) Dynamic structural evolution of overlying strata during shallow coal seam longwall mining. International Int J Rock Mech Min Sci 103:20–32

Wang F, Xu JL, Xie JL (2019) Effects of arch structure in unconsolidated layers on fracture and failure of overlying strata. Int J Rock Mech Min Sci 114:141–152

Wang G, Wu M, Wang R, Xu H, Song X (2017) Height of the mining-induced fractured zone above a coal face. Eng Geol 216:140–152

Wang J, Yang L, Li F, Wang C (2020a) Force chains in top coal caving mining. Int J Rock Mech Min Sci 127:104218

Wang S, Sun Q, Qiao J, Wang S (2020b) Geological guarantee of coal green mining. J China Coal Soc 45(1):8–15 (In Chinese)

Wang T, Zhou WB, Chen JH, Xiao X, Li Y, Zhao XY (2014) Simulation of hydraulic fracturing using particle flow method and application in a coal mine. Int J Coal Geol 121:1–13

Wang X, Zhang D, Zhang C, Fan G (2013) Mechanism of mining-induced slope movement for gullies overlaying shallow coal seams. J Mt Sci 10(3):388–397

Wu W, Bai J, Wang X, Zhu Z, Yan S (2019) Field investigation of fractures evolution in overlying strata caused by extraction of the jurassic and carboniferous coal seams and its application: case study. Int J Coal Geol 208:12–23

Xing H, Han Z (2020) Caving-induced fault reactivation behaviour and its effects on mining safety with a multiple seam context. Acta Geotech 15(12):3461–3481

Xu N, Zhang J, Tian H, Mei G, Ge Q (2016) Discrete element modeling of strata and surface movement induced by mining under open-pit final slope. Int J Rock Mech Min Sci 88:61–76

Xu Y, Wu K, Li L, Zhou D, Hu Z (2019) Ground cracks development and characteristics of strata movement under fast excavation: a case study at bulianta coal mine, china. Bull Eng Geol Environt 78(1):325–340

Yang TH, Xu T, Liu HY, Tang CA, Shi BM, Yu QX (2011) Stress-damage-flow coupling model and its application to pressure relief coal bed methane in deep coal seam. Int J Coal Geol 86(4):357–366

Yang X, Wen G, Dai L, Sun H, Li X (2019) Ground subsidence and surface cracks evolution from shallow-buried close-distance multi-seam mining: a case study in Bulianta coal mine. Rock Mech Rock Eng 52(8):2835–2852

Zhang T, Gan Q, Zhao Y, Zhu G, Nie X, Yang K, Li J (2019) Investigations into mining-induced stress-fracture-seepage field coupling effect considering the response of key stratum and composite aquifer. Rock Mech Rock Eng 52(10):4017–4031

Zhang YJ, Yan YG, Dai HY, Zhu YH, Wu TH (2021) Stability and force chain characteristics of "inclined step cutting body" in stope. Appl Sci 11:10276

Zhu X, Guo G, Liu H, Chen T, Yang X (2018) Experimental research on strata movement characteristics of backfill-strip ming using similar material modeling. Bull Eng Geol Environt 78(4):2151–2167